Impacts of dwarf mistletoe on the physiology of host Tsuga heterophylla trees as recorded in tree-ring C and O stable isotopes

Citation	Marias, D. E., Meinzer, F. C., Woodruff, D. R., Shaw, D. C., Voelker, S. L., Brooks, J. R., & Lachenbruch, B. (2014). Impacts of dwarf mistletoe on the physiology of host Tsuga heterophylla trees as recorded in tree-ring C and O stable isotopes. Tree Physiology, 34(6), 595-607. doi:10.1093/treephys/tpu046
DOI	10.1093/treephys/tpu046
Publisher	Oxford University Press
Version	Version of Record
Terms of Use	http://cdss.library.oregonstate.edu/sa-termsofuse

Tree Physiology 34, 595–607
doi:10.1093/treephys/tpu046

Research paper

Impacts of dwarf mistletoe on the physiology of host *Tsuga heterophylla* trees as recorded in tree-ring C and O stable isotopes

Danielle E. Marias[1,7], Frederick C. Meinzer[2], David R. Woodruff[2], David C. Shaw[3], Steven L. Voelker[4], J. Renée Brooks[5], Barbara Lachenbruch[1], Kristen Falk[3] and Jennifer McKay[6]

[1]Forest Ecosystems and Society, Oregon State University, 321 Richardson Hall, Corvallis, OR 97331, USA; [2]Pacific Northwest Research Station, USDA Forest Service, Corvallis, OR 97331, USA; [3]Forest Engineering, Resources and Management, Oregon State University, 280 Peavy Hall, Corvallis, OR 97331, USA; [4]Biology Department, Southern Oregon University, 1250 Siskiyou Blvd, Ashland, OR 97520, USA; [5]Western Ecology Division, US EPANHEERL, Corvallis, OR 97331, USA; [6]College of Earth, Oceanic, and Atmospheric Sciences, Oregon State University, 104 CEOAS Administration Building, Corvallis, OR 97331, USA; [7]Corresponding author (danielle.marias@oregonstate.edu)

Received September 18, 2013; accepted May 8, 2014; published online June 27, 2014; handling Editor Ram Oren

Dwarf mistletoes, obligate, parasitic plants with diminutive aerial shoots, have long-term effects on host tree water relations, hydraulic architecture and photosynthetic gas exchange and can eventually induce tree death. To investigate the long-term (1886–2010) impacts of dwarf mistletoe on the growth and gas exchange characteristics of host western hemlock, we compared the diameter growth and tree-ring cellulose stable carbon (C) and oxygen (O) isotope ratios ($\delta^{13}C_{cell}$, $\delta^{18}O_{cell}$) of heavily infected and uninfected trees. The relative basal area growth of infected trees was significantly greater than that of uninfected trees in 1886–90, but declined more rapidly in infected than uninfected trees through time and became significantly lower in infected than uninfected trees in 2006–10. Infected trees had significantly lower $\delta^{13}C_{cell}$ and $\delta^{18}O_{cell}$ than uninfected trees. Differences in $\delta^{18}O_{cell}$ between infected and uninfected trees were unexpected given that stomatal conductance and environmental variables that were expected to influence the $\delta^{18}O$ values of leaf water were similar for both groups. However, estimates of mesophyll conductance (g_m) were significantly lower and estimates of effective path length for water movement (L) were significantly higher in leaves of infected trees, consistent with their lower values of $\delta^{18}O_{cell}$. This study reconstructs the long-term physiological responses of western hemlock to dwarf mistletoe infection. The long-term diameter growth and $\delta^{13}C_{cell}$ trajectories suggested that infected trees were growing faster than uninfected trees prior to becoming infected and subsequently declined in growth and leaf-level photosynthetic capacity compared with uninfected trees as the dwarf mistletoe infection became severe. This study further points to limitations of the dual-isotope approach for identifying sources of variation in $\delta^{13}C_{cell}$ and indicates that changes in leaf internal properties such as g_m and L that affect $\delta^{18}O_{cell}$ must be considered.

Keywords: effective path length, mesophyll conductance.

Introduction

Dwarf mistletoe (*Arceuthobium* spp. Viscaceae) is an obligate, parasitic plant that primarily infects coniferous species and may eventually induce host tree death. Similar to leafy mistletoes (e.g., Loranthaceae), dwarf mistletoes acquire carbohydrates and water almost completely from host trees through haustorial connections to host xylem and phloem (Hawksworth and Wiens 1996). However, dwarf mistletoes differ considerably from leafy mistletoes in that they have diminutive, essentially leafless aerial shoots. Therefore, dwarf mistletoes are more heterotrophic (Hull and Leonard 1964, Logan et al. 2002) and have a miniscule transpiring shoot area compared with leafy mistletoes, which have a high transpiration rate per unit leaf area relative to that of host trees (Marshall et al. 1994*a*, 1994*b*, Zweifel et al. 2012).

As a result, the long-term negative impacts of dwarf mistletoes on tree growth and carbon (C) balance are likely to be indirect and related to disruption of water transport and consequent alterations in the hydraulic architecture and photosynthetic gas exchange rather than directly related to interception of water and fixed C. Water use of western hemlock (*Tsuga heterophylla* (Raf.) Sarg.) trees heavily infected with dwarf mistletoe (*Arceuthobium tsugense* (Rosendahl) G.N. Jones ssp. *tsugense*) was substantially less than that of co-occurring uninfected trees of similar size because infected trees exhibited branch dieback and reduced leaf area on surviving infected branches (Meinzer et al. 2004). Needle shedding on infected western hemlock branches conserved their leaf-specific conductivity despite sharply reduced hydraulic conductivity in spindle-shaped branch swellings (Meinzer et al. 2004). The predictable scaling of stomatal conductance (g_s) and photosynthesis (A) with leaf-specific conductivity (Hubbard et al. 2001, Santiago et al. 2004) suggests that photosynthetic gas exchange characteristics may be similar in needles on uninfected and infected trees. However, Sala et al. (2001) and Meinzer et al. (2004) observed reduced host leaf nitrogen (N) content, photosynthetic capacity (A_{max}) and intrinsic water-use efficiency (WUE, defined as the ratio A/g_s) in coniferous trees infected with dwarf mistletoe. These dwarf-mistletoe-induced alterations in photosynthetic gas exchange were recorded in stable C isotope ratios of needles on infected western hemlock branches (Meinzer et al. 2004).

Because dwarf mistletoe infections are initially localized and increase in severity over several decades, it is difficult to estimate when trees were initially infected and evaluate host physiological responses to the infection through time (Geils and Collazo 2002). Past growth responses of trees and their underlying physiological basis can often be characterized by concurrent analyses of tree-ring widths and stable isotopes of tree-ring cellulose, which record and integrate the impacts of physiology and the environment at the time the ring was formed (McCarroll and Loader 2004). Studies have shown that isotopic ratios of C and oxygen (O) of tree-ring cellulose ($\delta^{13}C_{cell}$, $\delta^{18}O_{cell}$) provide valuable information on plant C and water relations (Saurer et al. 1997, Barnard et al. 2012) and past environmental conditions (Roden et al. 2000, Brooks and Mitchell 2011). The $\delta^{13}C_{cell}$ and thus the C isotope discrimination, $\Delta^{13}C_{cell}$, reflect gas exchange by the plant at the time the C was fixed and can be used as a measure of intrinsic WUE (Farquhar et al. 1989*a*) unless disproportionate changes in mesophyll conductance (g_m) have occurred (Flexas et al. 2012).

However, it would also be useful to retrospectively separate the effects of variation in A and g_s on intrinsic WUE as indicated by $\Delta^{13}C_{cell}$. Concurrent analysis of $\delta^{18}O_{cell}$ has been proposed as an approach for separating variation in A and g_s because $\delta^{18}O_{cell}$ is only influenced by the water cycle, including g_s, and not A (Scheidegger et al. 2000). Variables influencing $\delta^{18}O_{cell}$ include the isotopic composition of source water, atmospheric water vapor, evaporative enrichment of leaf water (Roden et al. 2000, Barbour 2007) and a biochemical fractionation factor associated with incorporation of sugars into tree-ring cellulose (Yakir and DeNiro 1990). Transpiration (E) from the leaf is controlled by the leaf-to-air vapor pressure deficit (VPD) and stomatal and boundary layer conductances. Therefore, in co-occurring trees that rely on identical sources of water and experience similar relative humidity (RH) and VPD, differences in $\delta^{18}O_{cell}$ should result from differences in g_s and therefore E. However, studies have found that the use of the dual-isotope ($\delta^{13}C_{cell}$ and $\delta^{18}O_{cell}$) approach to compare treatment groups is complicated even when variables such as source water, water vapor, RH and T_{leaf} are similar among treatments (Brooks and Coulombe 2009).

Other factors also influence gas exchange and thus $\delta^{13}C_{cell}$ and $\delta^{18}O_{cell}$ besides A and g_s that are not accounted for by the dual-isotope approach, such as g_m and the length and tortuosity of the pathway from the xylem to the chloroplast and evaporative sites (effective path length, L) (Kahmen et al. 2008, Ferrio et al. 2012). These characteristics related to leaf anatomy may be influenced by the presence of dwarf mistletoe, which has been shown to alter water relations and hydraulic architecture (Meinzer et al. 2004), leaf size (Reblin et al. 2006) and leaf anatomy (Chhikara and Ross Friedman 2008) of host trees.

Although tree-ring C and O stable isotopes have been used to investigate the effect of insects on host physiology (Haavik et al. 2007, Simard et al. 2012), to our knowledge, the dual-isotope approach has not been used to evaluate the effect of a parasitic plant on the physiology of its host. To improve our understanding of the integrated effects of hemlock dwarf mistletoe on host physiology and photosynthetic gas exchange over time, we compared the annual radial growth, $\delta^{13}C_{cell}$ and $\delta^{18}O_{cell}$ of co-occurring uninfected and heavily infected old-growth western hemlock trees in southwestern Washington. We applied an established leaf water O isotope fractionation model and previous physiological measurements to estimate L and g_m to detect potential infection-induced changes in leaf anatomy (Roden et al. 2000, Barbour 2007). Based on previous measurements of photosynthetic gas exchange and leaf-specific hydraulic conductivity (Meinzer et al. 2004), we expected infected trees to have reduced radial growth, lower $\delta^{13}C_{cell}$ and similar $\delta^{18}O_{cell}$ compared to uninfected trees.

Materials and methods

Study species

Hemlock dwarf mistletoe (*A. tsugense*) infects western hemlock (*T. heterophylla*) along the west coast of North America from northern California to southeast Alaska (Hennon et al. 2001). Hemlock dwarf mistletoe is dioecious and produces

nectar-bearing flowers during mid–late summer. After pollination, fruits take 13–14 months to mature. Seeds are explosively discharged to horizontal distances up to 15 m from a single-seeded berry, causing dwarf mistletoe populations to be clumped based on stand composition. Once attached to a branch, the seed establishes a holdfast structure to develop its endophytic system and haustorial connections with host phloem and xylem (Hawksworth and Wiens 1996). Hemlock dwarf mistletoe induces localized branch infections visible as spindle-shaped swellings (Geils and Collazo 2002). Diminutive aerial shoots erupt from these swellings ~2–7 years after seed germination (Geils and Collazo 2002). Downstream from swellings, the host tree forms dense, fan-shaped branching systems called 'witches' brooms' that develop over a period of several years to decades.

Study area

The study site is located within a 4-ha plot in the T. T. Munger Research Natural Area in the Wind River Experimental Forest, in southwest Washington (45.820°N, 121.952°W) at an elevation of 368 m. Very wet winters and relatively dry summers characterize the climate. Average annual precipitation is 2176 mm with >90% falling during the rainy season of October–May (Carson Fish Hatchery, WA, USA; Western Regional Climate Center, Reno, NV; http://www.wrcc.dri.edu/). Average winter (December–March) and summer (June–September) temperatures are 2 and 16 °C, respectively. The stand selected for the study is dominated by old-growth western hemlock (~250 years old, 224 ha^{-1}) and Douglas-fir (*Pseudotsuga menziesii*, ~450 years old, 35 ha^{-1}). It was originally populated with Douglas-fir, a pioneer species, from 1500 to 1600 AD while western hemlock, a secondary successional species, was reproducing in the understory. Stand density is ~427 trees ha^{-1}.

Daily air temperature (T_{air}) and RH were recorded at the Wind River Canopy Crane Research Facility from 1999 to 2011 (University of Washington, http://depts.washington.edu/wrccrf/metdata/data/). Monthly estimates of precipitation, mean T_{air}, minimum air temperature (T_{min}), maximum air temperature (T_{max}) and dewpoint temperature were obtained from the PRISM Climate Group (Oregon State University, http://prism.oregonstate.edu). To obtain mean monthly daytime (0630–1930 h) T_{air} and RH for 1980–2010, monthly climate variables from PRISM for 1999–2011 were regressed against monthly on-site Wind River climate data ($y = 0.4715x + 10.892$, $y = 0.3191x + 40.715$, respectively) for the growing season that was considered to be May (day of year, DOY 121)–September (DOY 273). Vapor pressure deficit was estimated from T_{air} and dewpoint temperature using an algorithm for saturated vapor pressure (Paw and Gao, 1988). Monthly Palmer Drought Severity Index values were obtained for nearby Climate Divisions for Oregon and Washington from the IRI/LDEO climate data library (http://iridl.ldeo.columbia.edu/).

Assessment of dwarf mistletoe infection severity

All old-growth western hemlock trees at the site were surveyed for dwarf mistletoe infection severity using the Hawksworth six-class dwarf mistletoe rating (DMR) system (Hawksworth and Wiens 1996). Trees were inspected from the ground with binoculars. From observation, the crown is divided into thirds whereby each third is visually evaluated on a scale of 0–2: 0 is assigned to a third that displays 0% of branches infected, 1 for <50% infected and 2 for >50% infected. The sum of the 0–2 evaluations for each third is the DMR classification. Dwarf mistletoe rating 0 refers to uninfected trees and DMR 6 refers to heavily infected trees. Sampled heavily infected trees had significant signs of infection including formation of fan-shaped 'witches' brooms' and branch dieback.

Sampling

Thirteen uninfected (DMR 0, uninfected group) and 17 heavily infected (DMR 6, infected group) co-occurring western hemlock trees of approximately the same stem diameter (at 1.3-m height), age and tree height (Table 1) were sampled for growth and stable isotope analyses. Stem diameter and age were measured for all selected trees, whereas height was recorded for a subset of eight uninfected and nine infected trees. In July 2011, two 5-mm cores to pith and two 12-mm cores to ~10-cm depth at 180° from each other were extracted from each tree at ~1.3-m height. Cores were mounted, dried and sanded. Ring widths were measured using a sliding stage incremental micrometer (Velmex, Inc., Bloomfield, NY, USA) with Measure J2X software (VoorTech Consulting, Holderness, NH, USA). Visual cross-dating was verified using the COFECHA program to identify false or missing rings (Holmes 1983) for all cores collected. To compare rates of tree growth, ring-width data were converted to basal area increment (BAI, cm^2 $year^{-1}$) assuming a circular outline of stem cross-sections. To account for tree-size-related differences in growth during ontogeny, cross-dated BAI series were converted to relative basal area increment (RBAI). Relative basal area increment was calculated by dividing the BAI of a given year by the total basal area present during the previous year. For comparing inter-annual variability in growth to climate variables, the cross-dated ring-width series were detrended and standardized to produce ring-width index chronologies using the program ARSTAN (Cook and Holmes 1986). To create chronologies for each

Table 1. Stem diameter, age and height of western hemlock trees uninfected and infected with dwarf mistletoe. Values are means (±SE) of measurements made in 2011. Values followed by different letters within each column differ significantly at $P \leq 0.05$, $n = 8–17$.

	Diameter (cm)	Age (years)	Height (m)
Uninfected	91.3 ± 2.9a	225 ± 31.3a	52.1 ± 0.9a
Infected	90.6 ± 4.6a	210 ± 27.2a	48.8 ± 1.5a

of the DMR 0 and DMR 6 groups, each ring-width series was detrended twice with either a linear or a negative exponential regression in the first round to remove age-related trends. The second round of interactive detrending fit a flexible spline to each ring-width index series to remove trends associated with canopy disturbances. These methods result in a more coherent inter-annual climate signal for shade-tolerant tree species such as western hemlock that establish under closed canopy forest conditions and are often exposed to highly dynamic resource availability after canopy gap-formation disturbances (Cook 1985).

Sample preparation

Cores from a subset of six uninfected (DMR 0) and infected (DMR 6) trees that had ring widths closest to the mean per group were processed for stable isotope analysis for two different objectives. The first objective was to obtain a long-term $\delta^{13}C_{cell}$ record to evaluate potential shifts in physiology associated with mistletoe infection. Five-year groupings of annual growth rings alternating every 5 years were separated from the 5-mm cores along the entire core length, spanning over 100 years. Growth and C isotope data from cores collected in 2002 from three uninfected and two infected trees from the same stand (D.R. Woodruff, unpublished data) supplemented cores collected in 2011 for a total sample size of nine uninfected and eight infected trees analyzed in growth and long-term C isotope campaigns. Analyses with and without the 2002 cores were not significantly different (data not shown).

The second objective was to evaluate more recent physiological differences between the two DMR classes using both C and O isotopes. We used the shorter 12-mm cores, and selected two of the wettest and two of the driest years per decade spanning 1980–2010 for isotope analyses based on precipitation and temperature data. We expected dwarf-mistletoe-induced shifts in stomatal behavior and gas exchange to be most pronounced during drier years because they would pose the most extreme evaporative demands (McCarroll and Loader 2004). The two wettest years per decade selected from 1980 to 2010 included 1983, 1984, 1996, 1997, 2004 and 2010 and the dry years included 1987, 1989, 1992, 1999, 2006 and 2007. Each selected annual ring was separated with a razor blade and ground with a tissue homogenizer. All samples were extracted for alpha-cellulose. Oils and resins were removed with toluene–ethanol and ethanol Soxhlet extractions (Leavitt and Danzer 1993). Holocellulose was isolated by delignification in an acetic acid-acidified sodium chlorite solution and converted to alpha-cellulose in sodium hydroxide (Sternberg 1989).

Approximately 0.8 and 0.4 mg of alpha-cellulose were packed in tin and silver capsules for C combustion and O pyrolysis, respectively, for subsequent analysis by an isotope ratio mass spectrometer (IRMS). The C and O isotopic ratios were recorded as deviations per mil (‰) from the VPDB or VSMOW international standards, respectively.

Tree-ring cellulose from 5-year groupings was analyzed for $\delta^{13}C$ at Oregon State University's College of Earth, Oceanic, Atmospheric Sciences stable isotope laboratory. Samples were flash combusted using an elemental analyzer (NA 1500; Carlo Erba, Thermo Scientific, Waltham, MA, USA), and the resulting CO_2 was analyzed by continuous-flow IRMS using a Delta Plus XL (Finnigan MAT, now Thermo Scientific, Waltham, MA, USA) mass spectrometer. Runs were calibrated daily using the international standards USGS40 (glutamic acid) and ANU sucrose. The typical error was ±0.1‰ or better as determined by repeated measures of internal quality control standards (IAEA-600) and from sample replicates.

The $\delta^{13}C$ and $\delta^{18}O$ analyses of tree-ring cellulose from the selected wet and dry years were carried out at the University of California, Davis Stable Isotope Facility. Samples were analyzed for ^{13}C using an elemental analyzer (PDZ Europa ANCA-GSL, Sercon Ltd, Cheshire, UK) interfaced to an IRMS (PDZ Europa 20-20, Sercon Ltd). Samples were analyzed for ^{18}O using a combined pyrolysis/elemental analyzer (PyroCube, Elementar Analysensysteme GmbH, Hanau, Germany) interfaced to an IRMS (PDZ Europa 20-20, Sercon Ltd). Glutamic acid and alanine internal laboratory standards were used for order correction, size correction and elemental amounts. IAEA-601 and IAEA-602 benzoic acid were used for scale normalization. The typical error was ±0.2‰ or better as determined by repeated measures of internal quality control standards and from sample replicates.

Theory and modeling

To remove the impact of variation of $\delta^{13}C_{air}$ on $\delta^{13}C_{cell}$ values over time, $\delta^{13}C_{cell}$ values were converted to discrimination ($\Delta^{13}C$) using the following equation (Farquhar et al. 1982):

$$\Delta^{13}C_{cell} = \frac{\delta^{13}C_{air} - \delta^{13}C_{cell}}{1 + \delta^{13}C_{cell}}. \quad (1)$$

Values for $\delta^{13}C_{air}$ were obtained from the Scripps CO_2 Program (http://scrippsco2.ucsd.edu/) and McCarroll and Loader (2004). The $\Delta^{13}C$ of photosynthate reflects diffusional and biochemical fractionation against the heavier isotope during CO_2 fixation:

$$\Delta^{13}C = a + (b - a)\frac{c_i}{c_a}, \quad (2)$$

where a is the fractionation effect associated with diffusion of CO_2 through stomata (4.4‰), b is the fractionation effect (27‰) associated with discrimination against ^{13}C by the enzyme RUBISCO (ribulose bisphosphate carboxylase-oxygenase) during C fixation (Farquhar et al. 1982, 1989*b*)

and c_i/c_a is the weighted mean ratio of intercellular CO_2 concentration (c_i) to that in ambient air (c_a). Although Eq. (2) is a simplified form that does not account for other fractionation effects, it is sufficient for this application as $b = 27‰$ allows for a reduction in fractionation caused by omitted terms (Cernusak et al. 2013). However, $\Delta^{13}C_{cell}$ is higher (2–5‰) than that of the first products of photosynthesis due to other fractionation processes that occur during further metabolism (Leavitt and Long 1982). Nevertheless, tree-ring $\Delta^{13}C_{cell}$ reflects factors that influence discrimination against ^{13}C during photosynthetic CO_2 fixation. These factors include the biochemical capacity to fix CO_2 (A_{max}), and the conductance to CO_2 from the atmosphere to the sites of carboxylation, which includes the conductance to CO_2 from the atmosphere to intercellular spaces through stomata (g_s), as well as the conductance to CO_2 from the intercellular air spaces into the chloroplast through the mesophyll (g_m). Together, these conductances influence c_i and the CO_2 concentration at the sites of carboxylation (c_c), respectively. Thus, $\Delta^{13}C$ reflects the balance between the impacts of A_{max} and both g_s and g_m on C isotope discrimination, despite the fact that many models neglect the influence of g_m because g_s and g_m are often assumed to be correlated (Seibt et al. 2008, Flexas et al. 2012).

To estimate the relative impact of g_m on $\Delta^{13}C_{cell}$, we analyzed A–c_i curves measured on upper canopy branches of uninfected and infected western hemlock trees ($n = 3$) from the same stand in 2002 (Meinzer et al. 2004). The type of equation fit and parameters for infected and uninfected trees are shown in Table 2. The Sharkey et al. (2007) model was used to fit the A–c_i curves and to determine g_m.

Values of tree-ring $\delta^{18}O_{cell}$ incorporate a signal imparted by the $\delta^{18}O$ value of leaf water, which is mainly influenced by the $\delta^{18}O$ value of xylem water and ^{18}O enrichment at the sites of evaporation within the leaf (Craig and Gordon 1965, Dongmann et al. 1974). Under steady-state conditions,

$$\delta^{18}O_e = \delta^{18}O_s + \varepsilon^* + \varepsilon_k + (\delta^{18}O_v - \delta^{18}O_s - \varepsilon_k)\frac{e_a}{e_i}, \quad (3)$$

where $\delta^{18}O_e$, $\delta^{18}O_s$ and $\delta^{18}O_v$ represent the O isotopic composition of leaf water at the site of evaporation, source water (–10.0‰) and atmospheric water vapor (–18.0‰), respectively, e_a/e_i is the ratio of ambient vapor pressure to saturation vapor pressure within the leaf (affected by T_{leaf}), ε^* is the equilibrium fractionation between liquid water and vapor and ε_k is the kinetic fractionation factor of vapor diffusion from the leaf to the atmosphere. Values of $\delta^{18}O_s$ and $\delta^{18}O_v$ were measured at the same site during 2003 (F.C. Meinzer and J.R. Brooks, unpublished data) and 2011 (C.T. Lai, unpublished data), respectively, and used in the modeling exercise to put boundaries on possible ranges of the other parameters over several decades encompassed in the tree-ring chronologies.

Table 2. Parameters for A–c_i curves determined for western hemlock trees uninfected and infected with dwarf mistletoe and described by the equation $A = y_0 + a(1 - e^{-bx})$.

	Uninfected	Infected
y_0	–6.9602	–3.3173
a	35.7206	18.1075
b	0.0019	0.002

Leaf water isotopic heterogeneity can be explained further by the Péclet effect, which describes the ratio between the transpiration-induced mass flow (advection) of unenriched source water to the evaporative sites and the back diffusion of isotopically enriched water from the sites of evaporation (Farquhar and Lloyd 1993, Barbour 2007):

$$\delta^{18}O_{lw} = \delta^{18}O_e \frac{(1 - e^{-\wp})}{\wp}, \quad (4)$$

$$\wp = \frac{E\,L}{C\,D}, \quad (5)$$

where $\delta^{18}O_{lw}$ is the steady-state isotopic enrichment of mean leaf lamina water, $\wp$ is the Péclet number describing the ratio of advection to diffusion, E is the leaf transpiration rate (mol m^{-2} s^{-1}), L is the scaled effective path length (m) for water movement from the veins to the site of evaporation, C is the molar density of water (55.56×10^3 mol m^{-3}) and D is the diffusivity of the heavy water isotopologue ($H_2{}^{18}O$) in water (2.66×10^{-9} m^2 s^{-1}). L is defined as the product of two components: l, the actual distance of the water pathway from the xylem to the evaporative surface, and k, a scaling factor that accounts for the tortuosity of the path of water through a porous medium (Farquhar and Lloyd 1993, Barbour and Farquhar 2000, Cuntz et al. 2007).

Isotopic fractionation during the incorporation of the $\delta^{18}O_{lw}$ signal into cellulose of plant tissue is described by the following equation (Barbour and Farquhar 2000):

$$\delta^{18}O_{cell} = \delta^{18}O_{lw}\ (1 - p_{ex}p_x) + \varepsilon_o, \quad (6)$$

where p_{ex} is the proportion of O atoms that exchange with source water during cellulose formation (0.4), p_x is the proportion of unenriched water (xylem water) at the site of cellulose formation, which is equivalent to 1 for wood collected from the main trunk, and ε_o is a fractionation factor of +27‰ associated with the water/carbonyl interactions (Yakir and DeNiro 1990).

We used the Craig–Gordon model with the Péclet effect incorporated (Craig–Gordon Péclet model, Eq. (4), Barbour 2007) to estimate L for uninfected and infected trees using tree-ring $\delta^{18}O_{cell}$ from 1999, mean growing season (May–September) daytime RH, T_{air} and T_{leaf} (where $T_{leaf} = T_{air} + 1.5$ °C), and g_s

measured in 2002. T_{leaf} was assumed to be 1.5 °C greater than T_{air} because this is within the range that leaf temperature has often been shown to exceed air temperature in northern latitudes in conifers and other species (Martin et al. 1999, Helliker and Richter 2008). Estimates of L calculated with $T_{leaf} = T_{air}$ did not change the conclusions drawn from the results (data not shown). The year 2002 (when A–c_i curves were collected) was not selected for C and O isotope analyses and 1999 was the year selected for C and O isotope analyses that was closest to 2002 with similar climate conditions (T_{air}, RH, VPD; see Table S1 available as Supplementary Data at *Tree Physiology* Online). L was adjusted until the model prediction of $\delta^{18}O_{cell}$ matched the observed $\delta^{18}O_{cell}$. Transpiration was estimated from g_s measured diurnally (four to six sampling times/day, 0545–1640 h) on three branches of uninfected and infected western hemlock trees ($n = 3$) using a steady-state porometer (LI-1600; LiCor Inc., Lincoln, NE, USA) on 4 days during the 2002 growing season (see Figure S1 available as Supplementary Data at *Tree Physiology* Online) assuming that E of leaves enclosed in the ventilated porometer chamber reflected E of unenclosed leaves because the humidity balance point was set at the ambient value prior to each measurement and T_{leaf} in the chamber was close to T_{air}. The porometer measurements of g_s and E were therefore not independent because g_s was calculated based on E.

We also used the Craig–Gordon model with the Péclet effect to conduct a sensitivity analysis for values of g_s that would be required to yield the observed differences in $\delta^{18}O_{cell}$ between uninfected and infected trees at the values of L estimated for uninfected and infected trees. Climate variables (RH = 70% and T_{air} = 17 °C) when g_s was at its daily maximum (≅70 mmol m^{-2} s^{-1}; see Figure S1 available as Supplementary Data at *Tree Physiology* Online) were kept constant.

Statistical analyses

Simple linear regression was used to determine the slope and intercept of RBAI and $\Delta^{13}C_{cell}$ vs year, $\Delta^{13}C_{cell}$ vs $\delta^{18}O_{cell}$, and $\Delta^{13}C_{cell}$, $\delta^{18}O_{cell}$, and ring-width indices vs climate variables. Extra sum-of-squares F-tests were used to determine whether there was a significant interaction between group and year on RBAI, $\Delta^{13}C_{cell}$ and $\delta^{18}O_{cell}$. To determine differences in RBAI, $\Delta^{13}C_{cell}$ and $\delta^{18}O_{cell}$ between uninfected and infected trees, repeated-measures analysis was used with a compound symmetry correlation structure with tree as a grouping factor (significance level was $P \leq 0.05$). The model of best fit was selected based on Bayesian information criterion (BIC) values. Relative basal area increment was log transformed to meet model assumptions of equal variance and normality. However, for ease of interpretation, we present back-transformed data in results and figures. A two-sample t-test compared mean differences in tree diameter, height, age, $\Delta^{13}C_{cell}$, $\delta^{18}O_{cell}$, L, g_m and g_s between groups and $\Delta^{13}C_{cell}$ and $\delta^{18}O_{cell}$ between wet and dry years. Statistical analyses were conducted in SigmaPlot 12.3 (Systat Software, San Jose, CA, USA) and R version 2.15.2 (2012–10–26, The R Foundation for Statistical Computing). Error bars represent one standard error (SE).

Results

For the period 1876–2010, there was a significant interaction between group (i.e., uninfected and infected trees) and year on RBAI ($P = 0.0015$, Figure 1a) but not on $\Delta^{13}C_{cell}$ ($P = 0.29$, Figure 1b). The intercept (at year 1876) and rate of decline in RBAI in infected trees were significantly greater than those of uninfected trees ($P = 0.002$, 0.002, respectively, not shown). Relative basal area increment of infected trees was significantly greater than that of uninfected trees during 1886–90, 1956–60 and 1966–70 ($P = 0.02$, 0.01, 0.001, Figure 1a), while during 2006–10, infected trees had significantly lower RBAI than uninfected trees ($P = 0.005$, Figure 1a).

Infected trees had significantly greater $\Delta^{13}C_{cell}$ than uninfected trees during 1996–2000 and 2006–10 ($P = 0.01$,

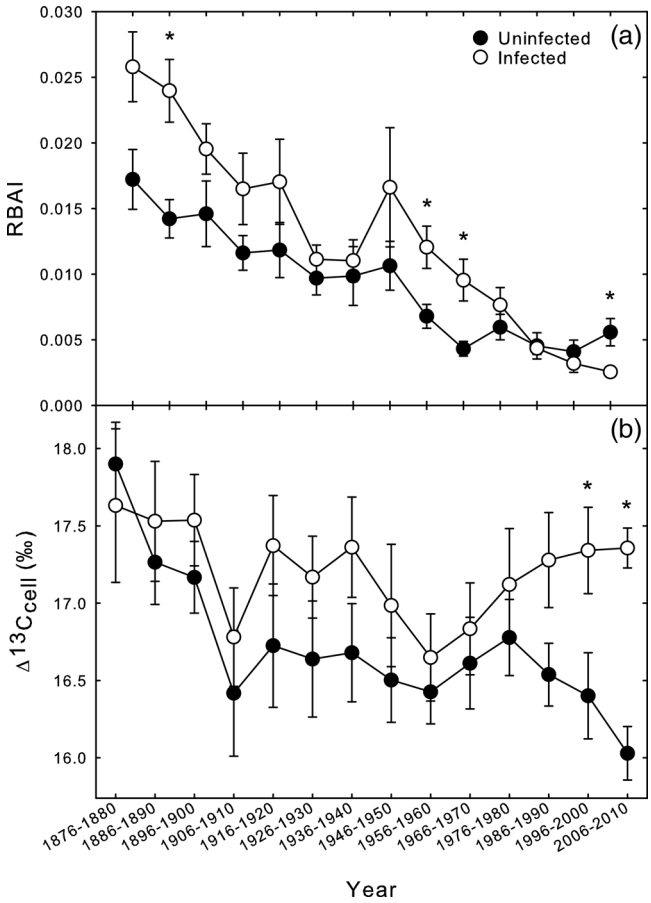

Figure 1. Mean ± SE of (a) 5-year RBAI and (b) 5-year $\Delta^{13}C_{cell}$ of uninfected (closed circles, $n = 9$) and infected (open circles, $n = 8$) trees for the period 1876–80 to 2006–10. Asterisks represent significant differences in repeated-measures analysis of variance ($P \leq 0.05$) between uninfected and infected trees.

0.03, Figure 1b). Mean $\Delta^{13}C_{cell}$ of uninfected trees was significantly lower in 2006–10 than in 1876–80 ($P = 0.002$), whereas $\Delta^{13}C_{cell}$ of infected trees did not display this trend over time ($P = 0.7$). Mean $\Delta^{13}C_{cell}$ of uninfected trees displayed a significant positive linear relationship with mean RBAI ($P = 0.001$, $r^2 = 0.6$, Figure 2). However, no significant relationship was found between RBAI and $\Delta^{13}C_{cell}$ of infected trees ($P = 0.3$, Figure 2), largely because of high $\Delta^{13}C_{cell}$ values in infected trees for the last few decades when RBAI was low. Contrary to expectations, correlations between ring widths and growing season climate variables were not significant for either group (see Table S2 available as Supplementary Data at *Tree Physiology* Online).

Analyses of $\Delta^{13}C_{cell}$ and $\delta^{18}O_{cell}$ for selected wet and dry years (Figure 3a and b) for the period 1980–2010 showed no interaction between group and year on $\Delta^{13}C_{cell}$ and $\delta^{18}O_{cell}$ of selected years ($P > 0.05$). $\Delta^{13}C_{cell}$ and $\delta^{18}O_{cell}$ values were not significantly different between wet and dry years for either group ($P > 0.05$). Consistent with the long-term 5-year $\Delta^{13}C_{cell}$ results (Figure 1b), infected trees had significantly greater mean $\Delta^{13}C_{cell}$ across all selected years during 1980–2010 where mean $\Delta^{13}C_{cell}$ was 16.5 ± 0.06‰ for uninfected trees and 17.8 ± 0.06‰ for infected trees ($P < 0.001$, Figure 3c).

Contrary to expectations that $\delta^{18}O_{cell}$ would be similar between groups, infected trees had significantly lower $\delta^{18}O_{cell}$ than uninfected trees across all selected years during 1980–2010, where mean $\delta^{18}O_{cell}$ was 26.0 ± 0.5‰ for uninfected trees and 23.8 ± 0.2‰ for infected trees ($P = 0.003$, Figure 3d). This trend was consistent in growth rings laid down in 1999, a year with similar climate conditions to 2002 (see Table 1 available as Supplementary Data at *Tree Physiology* Online) for which physiological data were available (see Figure S1 available as Supplementary Data at *Tree Physiology*

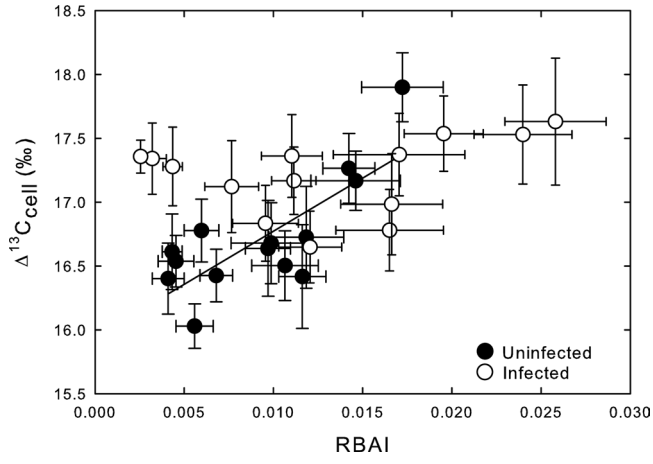

Figure 2. Mean ± SE of 5-year $\Delta^{13}C_{cell}$ in relation to RBAI of uninfected ($n = 9$) and infected trees ($n = 8$) for the period 1876–80 to 2006–10. RBAI and $\Delta^{13}C_{cell}$ were positively related in uninfected trees ($P = 0.001$, $r^2 = 0.6$) but not in infected trees.

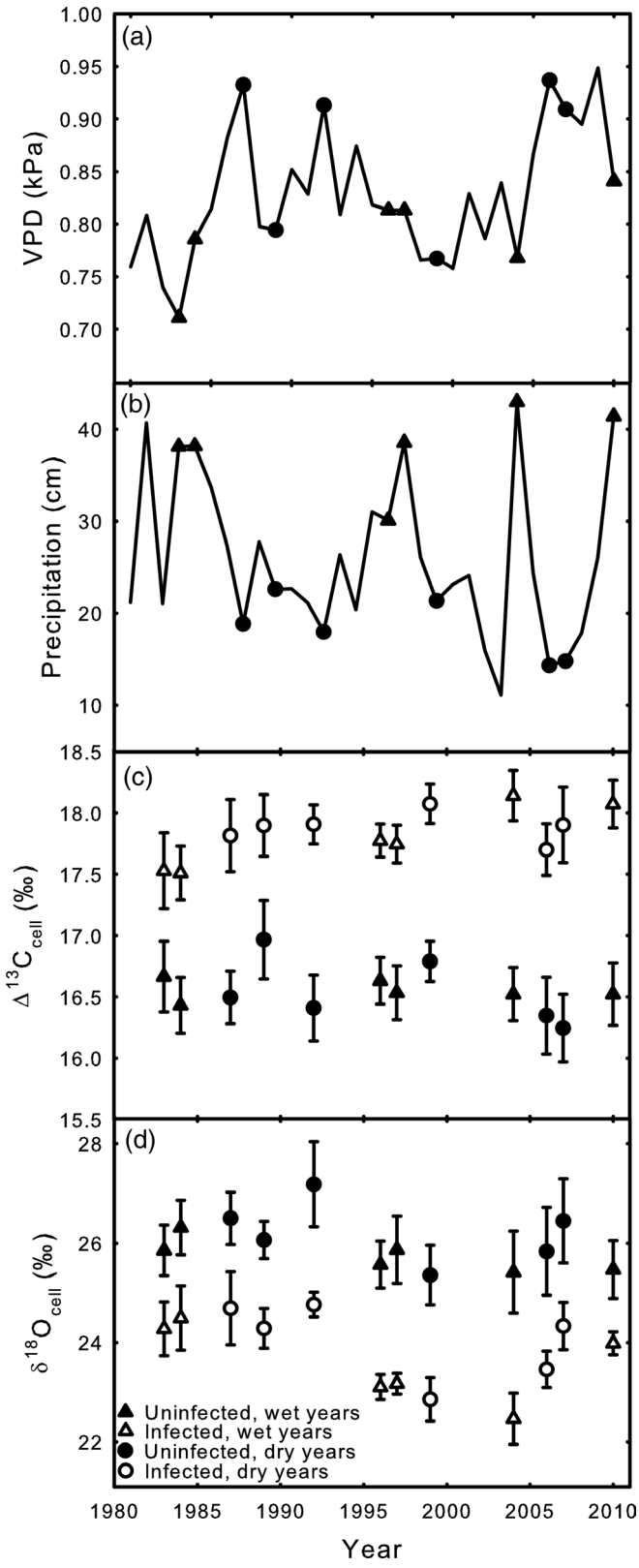

Figure 3. (a) Mean daytime (0630–1930 h) VPD, and (b) mean precipitation during the growing season (DOY 121–274) at the Wind River Field Station for two wet and two dry years per decade during the period 1980–10. Mean ± SE of (c) $\Delta^{13}C_{cell}$ and (d) $\delta^{18}O_{cell}$ of uninfected ($n = 6$) and infected ($n = 6$) trees for the 12 years represented in (a) and (b).

Table 3. Tree-ring $\Delta^{13}C_{cell}$ and $\delta^{18}O_{cell}$ for the year 1999, field measurements of g_s, and estimates of g_m and L of western hemlock trees uninfected and infected with dwarf mistletoe. Values are means (±SE). Values followed by different letters within each column differ significantly at $P \leq 0.05$, $n = 3–6$.

Condition	$\Delta^{13}C_{cell}$ (‰)	$\delta^{18}O_{cell}$ (‰)	g_s (mmol m^{-2} s^{-1})	g_m @ T_{leaf} (mmol m^{-2} s^{-1})	L (m)
Uninfected	16.8 ± 0.2a	25.4 ± 0.6a	29.2 ± 1.9a	56.0 ± 1.7a	0.12 ± 0.03a
Infected	18.1 ± 0.2b	22.9 ± 0.2b	33.4 ± 2.7a	39.1 ± 5.3b	0.35 ± 0.02b

Online and $A–c_i$ curves, Figure 6 in Meinzer et al. 2004). In 1999, mean $\delta^{18}O_{cell}$ was 25.4 ± 0.6‰ for uninfected trees and 22.9 ± 0.2‰ for infected trees (Table 3), despite diurnal g_s measured in 2002 (see Figure S1 available as Supplementary Data at *Tree Physiology* Online) and therefore E not being significantly different between uninfected and infected trees ($P = 0.36$).

If differences in E and g_s were not likely responsible for the changes in $\delta^{18}O_{cell}$ we observed, and source water and climate variables were the same between the two groups, the last possible variable in Eq. (5) was L, the effective path length. Infected trees had significantly lower g_m than uninfected trees (Table 3) based on 2002 gas exchange measurements (see $A–c_i$ curves in Figure 6 in Meinzer et al. 2004), suggesting the presence of internal differences in leaf structure that could also influence L. Using the 2002 measured g_s (see Figure S1 available as Supplementary Data at *Tree Physiology* Online), climate variables (T_{air} and RH; see Figure S1 and Table S1 available as Supplementary Data at *Tree Physiology* Online) and the 1999 $\delta^{18}O_{cell}$ (Table 3) in the Craig–Gordon Péclet model, we estimated that L in infected trees was approximately three times greater than that in uninfected trees ($P \leq 0.05$, Table 3).

Also contrary to expectations, values between wet and dry years (Figure 3a and b) for both $\Delta^{13}C_{cell}$ and $\delta^{18}O_{cell}$ were similar within uninfected and infected groups ($P = 0.20–0.94$). Nevertheless, for the uninfected trees, correlations between $\Delta^{13}C_{cell}$ and growing season T_{air}, RH and VPD were significant (see Table S3 available as Supplementary Data at *Tree Physiology* Online). For the infected trees, correlations between $\Delta^{13}C_{cell}$ and growing season climate variables were not significant (see Table S3 available as Supplementary Data at *Tree Physiology* Online). Correlations between $\delta^{18}O_{cell}$ and growing season climate variables were not significant for either group (see Table S3 available as Supplementary Data at *Tree Physiology* Online).

There was a significant negative linear relationship between mean $\Delta^{13}C_{cell}$ and $\delta^{18}O_{cell}$ across uninfected and infected trees ($P < 0.001$, $r^2 = 0.68$, Figure 4), although within each group the relationship was not significant for either group ($P = 0.6$ and 0.8 for uninfected and infected trees, respectively).

The sensitivity analysis (Figure 5) predicted that for L values of 0.354 m estimated for infected trees and 0.118 m estimated for uninfected trees, g_s of infected trees would have to be 175–200 mmol m^{-2} s^{-1}, more than twice as high as the measured

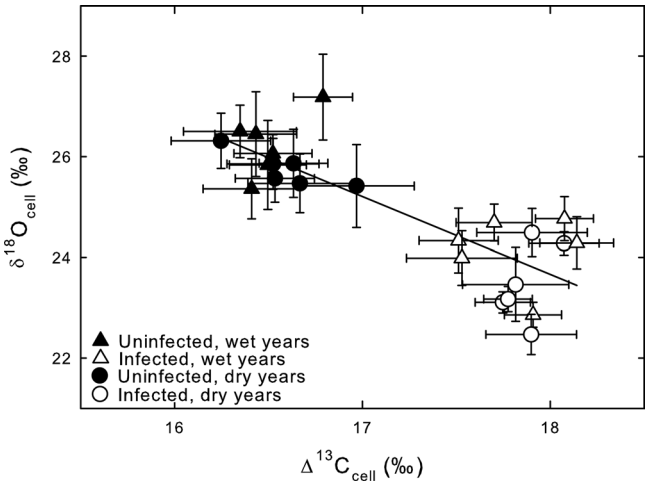

Figure 4. Mean ± SE $\delta^{18}O_{cell}$ in relation to $\Delta^{13}C_{cell}$ of uninfected ($n = 6$) and infected ($n = 6$) trees for six wet and six dry years during the period 1980–2010. $\Delta^{13}C_{cell}$ and $\delta^{18}O_{cell}$ were negatively related across uninfected and infected trees ($P < 0.001$, $r^2 = 0.68$), although within each group, the relationship was not significant for either group ($P = 0.6$, 0.8).

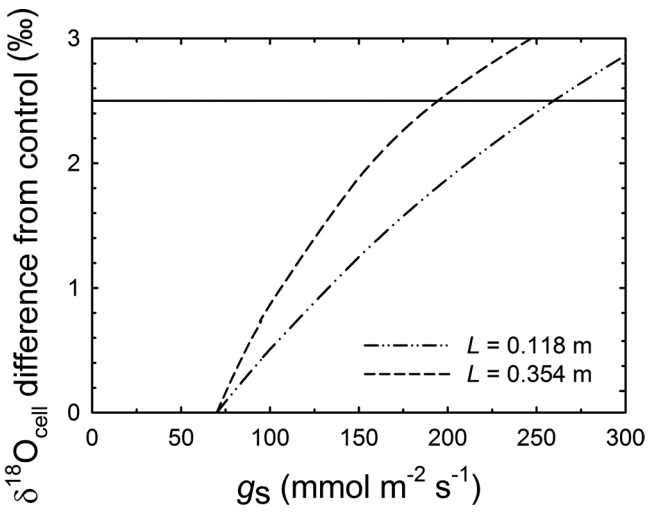

Figure 5. Modeled relationship between g_s and the resulting difference in $\delta^{18}O_{cell}$ between uninfected control trees ($g_s = 70$ mmol m^{-2} s^{-1}) and infected trees following Eq. (3–6). Curved lines represent estimated effective path lengths (L) for infected (0.354 m) and uninfected (0.118 m) trees. The horizontal line represents the observed difference in $\delta^{18}O_{cell}$ between uninfected and infected trees. The simulation predicts that for the range of L shown, g_s of infected trees would have to be more than twice as high as the measured maximum daily g_s, 175–200 mmol m^{-2} s^{-1}, to account for the observed difference in $\delta^{18}O_{cell}$ between the two groups.

maximum daily g_s (70 mmol m^{-2} s^{-1}; see Figure S1 available as Supplementary Data at *Tree Physiology* Online), to account for the observed 2.5‰ difference in $\delta^{18}O_{cell}$ between the two groups (horizontal line, Figure 5).

Discussion

The integrated effects of long-term dwarf mistletoe infection on host western hemlock trees were recorded in the radial growth, $\Delta^{13}C_{cell}$ and $\delta^{18}O_{cell}$ of tree-rings. The radial growth and $\Delta^{13}C_{cell}$ trajectories described the intensification of dwarf mistletoe infection throughout host tree crowns. During the most recent decades, heavily infected western hemlock trees had lower RBAI and greater $\Delta^{13}C_{cell}$ than uninfected trees, consistent with previous studies of the effects of dwarf mistletoe on host radial growth and physiology (Meinzer et al. 2004, Shaw et al. 2008, Logan et al. 2012). However, the significantly lower $\delta^{18}O_{cell}$ in infected than uninfected trees was not explained by elements of O isotope theory that attribute variation in $\delta^{18}O_{cell}$ to factors such as climate, source water and transpiration. This was also not explained by the dual-isotope approach typically used to estimate relative stomatal limitation of *A* using relationships between $\Delta^{13}C_{cell}$ and $\delta^{18}O_{cell}$. Because dwarf mistletoe has been shown to impact host water relations and hydraulic architecture (Meinzer et al. 2004), and leaf size and anatomy (Reblin et al. 2006, Chhikara and Ross Friedman 2008), we used the Craig–Gordon Péclet model and A–c_i curves to estimate L and g_m speculating that these leaf internal parameters could be driving the observed $\delta^{18}O_{cell}$ patterns.

Growth and $\Delta^{13}C_{cell}$

The combination of radial growth and $\Delta^{13}C_{cell}$ analyses illustrated the initial intensification of dwarf mistletoe infection in tree crowns and the cumulative impact of the infection through time (Figure 1). The RBAI of trees that became infected declined more rapidly than in trees that remained uninfected, suggesting that symptoms such as branch dieback and subsequent reductions in leaf area, needle N content and A_{max} resulted in reduced radial growth as dwarf mistletoe intensified in the crown through time and persisted as a nutrient sink (Flanagan et al. 1993, Marshall et al. 1994*a*, 1994*b*, Cernusak et al. 2004, Meinzer et al. 2004, Bickford et al. 2005). By 2006–10, the RBAI of infected trees was significantly lower than that of uninfected trees, consistent with other reports of reduced radial growth in severely infected trees (Shaw et al. 2008, Logan et al. 2012).

Trajectories of RBAI indicated that infected trees were growing faster than uninfected trees prior to becoming infected (Figure 1a). Consistent with this observation, Shaw et al. (2005) and Stanton (2007) hypothesized that larger, more vigorously growing trees are more likely to become infected. This may be due to the presence of a greater amount of branch area to intercept seed rain from explosive dehiscence and from animal vectored dispersal (Geils and Collazo 2002). Larger trees also intercept more sunlight than smaller mid-story trees, satisfying high light requirements for aerial shoot production (Shaw and Weiss 2000). Host *Pinus ponderosa* water and nutrient status has been shown to be positively correlated with dwarf mistletoe (*Arceuthobium vaginatum* subsp. *cryptopodum*) growth, suggesting that dwarf mistletoe robustness initially depends on host vigor (Bickford et al. 2005). Larger, more vigorously growing trees are more likely to survive longer with the dwarf mistletoe infection and become heavily infected.

Significantly greater RBAI of infected trees in 1956–60 and 1966–70 (Figure 1a) may have been associated with the formation of witches' brooms and a transient increase in host photosynthetic leaf area (Sala et al. 2001) resulting in greater radial growth than that observed in uninfected trees. The formation of witches' brooms is believed to be due to dwarf-mistletoe-induced alterations in growth-regulating hormones such as cytokinins (Logan et al. 2012). However, needle loss ultimately occurs downstream from the localized infections apparently as a result of hydraulic occlusions caused by sinkers and haustorial connections (Wilson and Calvin 1996, Meinzer et al. 2004). Although needle shedding appears to compensate for this hydraulic bottleneck by maintaining leaf-specific conductivity, interception of N by the mistletoe reduces the photosynthetic capacity of the remaining needles (Meinzer et al. 2004). Consequently, the remaining foliage would not be able to support the respiratory demands of the increased branch area and volume of witches' brooms, resulting in cumulative branch dieback that contributes to significant reductions in radial growth observed in trees with severe long-term infections.

Concurrent with significantly lower radial growth in 2006–10 in infected than uninfected trees, $\Delta^{13}C_{cell}$ was significantly greater in infected trees during 2006–10 (Figure 1b). Because g_s was not significantly different between the two groups (see Figure S1 available as Supplementary Data at *Tree Physiology* Online), the greater $\Delta^{13}C_{cell}$ in infected trees (Figure 1b) was presumably caused by an increase in c_c likely due to significantly lower needle N content and lower A_{max} measured in heavily infected western hemlock trees relative to uninfected trees in this stand (Meinzer et al. 2004). Climate-related changes in g_s did not have an appreciable effect on $\Delta^{13}C$ due to diminished A_{max}, explaining the lack of significant relationships between climate variables and $\Delta^{13}C$ in infected trees (see Table S3 available as Supplementary Data at *Tree Physiology* Online). Needles of trees infected with dwarf mistletoe have also been shown to have greater $\Delta^{13}C$ values than those of uninfected trees (Sala et al. 2001, Meinzer et al. 2004, Logan et al. 2012), demonstrating that fractionation events that influence $\Delta^{13}C$ at the leaf level are reflected in $\Delta^{13}C_{cell}$ of tree-rings (Leavitt and Long 1982).

Interestingly, these concurrent differences in RBAI and $\Delta^{13}C_{cell}$ between groups in tree-rings did not become apparent until 1996–2000 and 2006–10, suggesting that several decades were required for the effects of dwarf mistletoe on the physiology of infected trees to be recorded in tree-rings. In previous work at the Wind River site, Shaw et al. (2008) found that the growth rates of lightly and moderately infected western hemlock trees did not significantly differ from those of uninfected trees, but the growth rates of severely infected trees were 16–46% lower than those of uninfected trees.

Generally, $\Delta^{13}C$ of leaf tissue and thus $\Delta^{13}C_{cell}$ decrease with increasing tree height (Woodruff et al. 2009, McDowell et al. 2011). Since RBAI also decreases with increasing tree size and height, tree-ring $\Delta^{13}C_{cell}$ should decrease concurrently. Only uninfected trees displayed the expected relationship between $\Delta^{13}C_{cell}$ and RBAI (Figure 2). In severely infected trees, significantly greater tree-ring $\Delta^{13}C_{cell}$ between 1980 and 2010 (Figure 3) caused the relationship between $\Delta^{13}C_{cell}$ and RBAI to deviate from the expected relationship observed in uninfected trees (Figure 2).

The biology and development of the pathogen make it almost impossible to determine an exact year when trees were infected. *Arceuthobium tsugense* produces localized infections only in branches on which its seeds germinate and the plants become established. Therefore, it takes years/decades for *A. tsugense* to mature and disperse its seed to gradually infect nearly the entire crown. We can speculate that the infected trees we studied reached that critical threshold when $\Delta^{13}C_{cell}$ of infected trees became significantly greater than that of uninfected trees in 1996–2000. However, it is well documented (Shaw et al. 2005, 2008) that dwarf mistletoe can take several decades before trees are considered severely infected enough to reach a DMR of 6. Thus, the DMR 6 trees in our study could have been initially infected before or during 1946–50 despite no significant difference in RBAI or $\Delta^{13}C_{cell}$.

$\delta^{18}O_{cell}$

Variation in $\delta^{18}O_{cell}$ can be explained by environmental conditions (e.g., source water and RH) and leaf physiological (g_s and E) and structural characteristics (e.g., L, g_m). However, using the dual-isotope approach (Scheidegger et al. 2000), differences in $\delta^{18}O_{cell}$ across treatment groups under similar environmental conditions are interpreted as being driven largely by changes in g_s because g_s regulates E, evaporative enrichment of leaf water and thus $\delta^{18}O_{cell}$. Therefore, we had hypothesized that $\delta^{18}O_{cell}$ of infected and uninfected trees would not differ because field measurements showed that g_s of these co-occurring trees was not significantly different (see Figure S1 available as Supplementary Data at *Tree Physiology* Online). Contrary to our hypothesis, infected trees had significantly lower $\delta^{18}O_{cell}$ than uninfected trees regardless of fluctuations in climate (Figure 3), and measurements of g_s were not different between the groups (Table 3). To explain the unexpected differences in $\delta^{18}O_{cell}$ between uninfected and infected groups, we used the Craig–Gordon Péclet model to estimate values of L of uninfected and infected trees that would result in their observed differences in $\delta^{18}O_{cell}$. Our results suggested that leaf structural characteristics (e.g., L, g_m) rather than g_s, climate or differences in how trees responded to climate may explain the observed variation in $\delta^{18}O_{cell}$. Our estimated values of L for uninfected and infected trees (Table 3) are consistent with previously published values of L for conifers (Song et al. 2013). The sensitivity analysis of g_s and $\delta^{18}O_{cell}$ at the estimated values of L (Figure 5) suggests that to yield the observed differences in $\delta^{18}O_{cell}$ between groups, values of g_s for infected trees would have to be unrealistically high compared with those measured in large, old-growth trees of western hemlock and other conifers. Typical values of g_s of old-growth western hemlock measured in this stand range from 36 to 156 mmol m^{-2} s^{-1} (J.M. Warren, unpublished data), consistent with measured g_s values in Figure S1 available as Supplementary Data at *Tree Physiology* Online. In contrast to the measured values of g_s, the simulation predicted that for the range of L shown, g_s of infected trees would have to be 175–250 mmol m^{-2} s^{-1} to account for the observed 2.5‰ difference in $\delta^{18}O_{cell}$ between the two groups (Figure 5). Thus, the sensitivity analysis in addition to field measurements of g_s at the study site suggested that differences in g_s were not the primary drivers behind the differences in $\delta^{18}O_{cell}$ between uninfected and infected trees.

Many studies using the dual-isotope approach have attributed variation in $\delta^{18}O_{cell}$ to tree responses to climatic variables such as RH and VPD (Saurer et al. 1997, Scheidegger et al. 2000, Barbour et al. 2002), thinning and fertilization treatments that altered crown microclimate (Brooks and Coulombe 2009, Brooks and Mitchell 2011), and seasonal changes in precipitation (Roden and Ehleringer 2007). However, we ruled out differences in source water and microclimate as major drivers behind the observed differences in $\delta^{18}O_{cell}$ because uninfected and infected trees were growing in the same stand and experiencing similar environmental conditions over time. Furthermore, the differences between groups were consistent regardless of annual climatic variations (Figure 3). The trees sampled were also similar in age and size at the time of the study (Table 1) and were infected decades after root systems were developed. Therefore, it is unlikely that uninfected and infected trees were accessing water at different depths (Brooks et al. 2006).

In addition, ring-width indices and $\delta^{18}O_{cell}$ were not significantly correlated with climate variables for either group (see Tables S2 and S3 available as Supplementary Data at *Tree Physiology* Online). This result implies that the majority of photosynthate eventually incorporated into tree-ring cellulose was fixed into sugars when g_s was highest prior to substantial diurnal decreases in RH and increases in VPD and T_{air} (see Figure S1 available as Supplementary Data at *Tree Physiology* Online).

At high RH and therefore low evaporative demand, ^{18}O enrichment is relatively insensitive to large variation in g_s (Barbour and Farquhar 2000). This is consistent with the lack of relationship between $\Delta^{13}C_{cell}$ and $\delta^{18}O_{cell}$ within each group (Figure 4) and with field measurements of g_s (see Figure S1 available as Supplementary Data at *Tree Physiology* Online), suggesting that infected trees lacked stomatal adjustment in response to reduced A_{max} (Meinzer et al. 2004).

After ruling out climate and g_s as primary drivers behind the significant difference in $\delta^{18}O_{cell}$ between uninfected and infected trees, we considered g_m and L, which are related to leaf anatomical characteristics that impact both parameters as CO_2 and H_2O have overlapping pathways in the leaf (Ferrio et al. 2012). Few studies have quantified the effects of dwarf mistletoe on host leaf anatomy. Chhikara and Ross Friedman (2008) found that vascular bundles of *Pinus contorta* needles downstream of dwarf mistletoe infections were positioned significantly closer together than in needles of uninfected trees, but the implications of these findings for species such as western hemlock whose needles contain a single vascular bundle are unclear. Previous work has shown that g_m is positively correlated with A_{max} under non-saturating CO_2 concentrations (Flexas et al. 2008), consistent with lower A_{max} and g_m observed in infected western hemlock trees (Table 3, Meinzer et al. 2004). L accounts for both the length and tortuosity of the pathway of water movement from the xylem to the evaporative sites, which influences evaporative enrichment of leaf water and ultimately $\delta^{18}O_{cell}$ (Kahmen et al. 2008, Ferrio et al. 2012, Song et al. 2013). Because the transport pathways for CO_2, water vapor and liquid water overlap, it is not surprising that estimates of L and g_m are inversely related (Ferrio et al. 2012), consistent with our findings that infected trees had estimated values of L roughly three times greater than uninfected trees and values of g_m that were ~34% lower than uninfected trees (Table 3).

These findings suggest that differences between infected and uninfected trees in leaf characteristics related to L and g_m were stronger drivers of differences in $\delta^{18}O_{cell}$ than variation in g_s, E and related environmental drivers, consistent with previous work (Kahmen et al. 2008, Ferrio et al. 2012, Song et al. 2013). The degree of coordination between g_m and g_s and the relative contribution of g_m to the limitation of A_{max} and its co-regulation with g_s must be considered when interpreting $\Delta^{13}C_{cell}$ and WUE, often used to predict how trees may respond to future shifts in climate (Sangüesa-Barreda et al. 2013). Additional investigations of the relationship between L and g_m may improve interpretations of the physiological and structural attributes that contribute to variation in $\Delta^{13}C_{cell}$ and $\delta^{18}O_{cell}$. Future studies should investigate the effect of the dwarf mistletoe infection on leaf anatomical characteristics that influence L and g_m such as mesophyll cell wall thickness and the positioning of vascular bundles in relation to sites of evaporation as well as direct measurements of leaf water enrichment in co-occurring uninfected and infected trees (Terashima et al. 2006, Lambers et al. 2008).

Conclusions

Combined trends of radial growth and $\Delta^{13}C_{cell}$ were useful metrics for tracking the intensification of the dwarf mistletoe infection through time, particularly for detecting the threshold at which trees displayed significant physiological impacts of the infection. Because impacts of the infection on radial growth and $\Delta^{13}C_{cell}$ were evident only at advanced stages of infection, we could not identify exactly when trees became infected. Although the dual-isotope approach is a useful tool, our results also point to the limitations of the dual-isotope approach (Scheidegger et al. 2000) for identifying sources of variation in c_i/c_a and therefore $\Delta^{13}C_{cell}$ (Roden and Farquhar 2012, Roden and Siegwolf 2012) because it does not account for the physiological effects of pathogens or variation in leaf anatomical characteristics that affect L and g_m, and ultimately $\delta^{18}O_{cell}$ in the absence of changes in g_s. Our findings have important implications for reconstructing tree responses to climate fluctuations because undetected dwarf mistletoe or other pathogens that modify leaf anatomy and functioning may imprint an unknown degree of variability on stable isotope signatures presumed to be driven by climatic variation. Studies integrating leaf to whole-tree physiology will improve our understanding of the western hemlock–dwarf mistletoe system from the tree to the canopy, especially because ecosystem-scale effects of dwarf mistletoe are still being explored (Watson 2001, Shaw et al. 2004, Bell and Adams 2011, Way 2011).

Supplementary data

Supplementary data for this article are available at *Tree Physiology* online.

Acknowledgments

The authors thank Brandy Saffell for her help with field and lab work and John Roden for his comments on an earlier version of the manuscript. The Wind River Field Station (WRFS), formerly the Wind River Canopy Crane Research Facility, provided excellent logistical support. The WRFS is a joint venture among the University of Washington, the USDA Forest Service Pacific Northwest Research Station and the Gifford Pinchot National Forest. The authors also thank Chun-Ta Lai for providing water vapor isotope data. This manuscript has been subjected to the Environmental Protection Agency's peer and administrative review, and it has been approved for publication as an EPA document. Mention of trade names or commercial products does not constitute endorsement or recommendation for use.

Conflict of interest

None declared.

Funding

Financial support was provided by the National Science Foundation under award number DEB-0743882.

References

Barbour MM (2007) Stable oxygen isotope composition of plant tissue: a review. Funct Plant Biol 34:83–94.

Barbour MM, Farquhar GD (2000) Relative humidity- and ABA-induced variation in carbon and oxygen isotope ratios of cotton leaves. Plant Cell Environ 23:473–485.

Barbour MM, Walcroft AS, Farquhar GD (2002) Seasonal variation in $\delta^{13}C$ and $\delta^{18}O$ of cellulose from growth rings of *Pinus radiata*. Plant Cell Environ 25:1483–1499.

Barnard HR, Brooks JR, Bond BJ (2012) Applying the dual-isotope conceptual model to interpret physiological trends under uncontrolled conditions. Tree Physiol 32:1183–1198.

Bell TL, Adams MA (2011) Attack on all fronts: functional relationships between aerial and root parasitic plants and their woody hosts and consequences for ecosystems. Tree Physiol 31:3–15.

Bickford CP, Kolb TE, Geils BW (2005) Host physiological condition regulates parasitic plant performance: *Arceuthobium vaginatum* subsp. *cryptopodum* on *Pinus ponderosa*. Oecologia 146:179–189.

Brooks JR, Coulombe R (2009) Physiological responses to fertilization recorded in tree-rings: isotopic lessons from a long-term fertilization trial. Ecol Appl 19:1044–1060.

Brooks JR, Mitchell AK (2011) Interpreting tree responses to thinning and fertilization using tree-ring stable isotopes. New Phytol 190:770–782.

Brooks JR, Meinzer FC, Warren JM, Domec JC, Coulombe R (2006) Hydraulic redistribution in a Douglas-fir forest: lessons from system manipulations. Plant Cell Environ 29:138–150.

Cernusak LA, Pate JS, Farquhar GD (2004) Oxygen and carbon isotope composition of parasitic plants and their hosts in southwestern Australia. Oecologia 139:199–213.

Cernusak LA, Ubierna N, Winter K, Holtum JAM, Marshall JD, Farquhar GD (2013) Environmental and physiological determinants of carbon isotope discrimination in terrestrial plants. New Phytol 200:950–965.

Chhikara A, Ross Friedman CM (2008) The effects of male and female *Arceuthobium americanum* (lodgepole pine dwarf mistletoe) infection on the relative positioning of vascular bundles, starch distribution, and starch content in *Pinus contorta* var. *latifolia* (lodgepole pine) needles. Botany 86:539–543.

Cook ER (1985) A time series approach to tree-ring standardization. Ph.D. dissertation, University of Arizona, Tucson AZ, 171 p.

Cook ER, Holmes RL (1986) User's manual for Oorogram ARSTAN. Laboratory of Tree-Ring Research, University of Arizona, Tucson, AZ.

Craig H, Gordon LI (1965) Deuterium and oxygen-18 variation in the ocean and the marine atmosphere. In: Tongiorgi E (ed) Proceedings of a conference on stable isotopes in oceanographic studies and paleotemperatures. Spoleto, Italy, pp 9–130.

Cuntz M, Ogee J, Farquhar GD, Peylin P, Cernusak LA (2007) Modelling advection and diffusion of water isotopologues in leaves. Plant Cell Environ 30:892–909.

Dongmann G, Nurnberg HW, Forstel H, Wagener K (1974) On the enrichment of $H_2{}^{18}O$ in the leaves of transpiring plants. Radiat Environ Biophys 11:41–52.

Farquhar GD, Lloyd J (1993) Carbon and oxygen isotope effects in the exchange of carbon dioxide between terrestrial plants and the atmosphere. In: Ehleringer JR, Hall AE, Farquhar GD (eds) Stable isotopes and plant carbon–water relations. Academic Press, San Diego, pp 47–70.

Farquhar GD, O'Leary MH, Berry JA (1982) On the relationship between carbon isotope discrimination and the intercellular carbon dioxide concentration in leaves. Aust J Plant Physiol 9:121–137.

Farquhar GD, Hubick KT, Condon AG, Richards RA (1989*a*) Carbon isotope fractionation and plant water-use efficiency. In: Rundel PW, Ehleringer JR, Nagy KA (eds) Stable isotopes in ecological research. Springer, Berlin, pp 21–40.

Farquhar GD, Ehleringer JR, Hubick KT (1989*b*) Carbon isotope discrimination and photosynthesis. Annu Rev Plant Physiol Plant Mol Biol 40:503–537.

Ferrio JP, Pou A Florez-Sarasa I, Gessler A, Kodama N, Flexas J, Ribas-Carbo M (2012) The Péclet effect on leaf water enrichment correlates with leaf hydraulic conductance and mesophyll conductance for CO2. Plant Cell Environ 35:611–625.

Flanagan LB, Marshall JD, Ehleringer JR (1993) Photosynthetic gas exchange and the stable isotope composition of leaf water: comparison of a xylem-tapping mistletoe and its host. Plant Cell Environ 16:623–631.

Flexas J, Ribas-Carbo M, Diaz-Espejo A, Galmes J, Medrano H (2008) Mesophyll conductance to CO_2: current knowledge and future prospects. Plant Cell Environ 31:602–621.

Flexas J, Barbour MM, Brendel O et al. (2012) Mesophyll diffusion conductance to CO2: An unappreciated central player in photosynthesis. Plant Sci 193–194:70–84.

Geils BW, Collazo IV (2002) Loranthaceae and Viscaceae in North America. In: Geils BW, Tovar JC, Moody B (eds) Mistletoes of North American Conifers. General Technical Report RMRS GTR-98. USDA Forest Service, pp 1–5.

Haavik LJ, Stephen FM, Fierke MK, Salisbury VB, Leavitt SW, Billings SA (2007) Dendrochronological parameters of northern red oak infested with red oak borer. For Ecol Manag 255:1501–1509.

Hawksworth, FG, Wiens D (1996) Dwarf mistletoes: biology, pathology and systematics. Agriculture Handbook 709. USDA Forest Service, Washington, DC, 410 p.

Helliker BR, Richter SL (2008) Subtropical to boreal convergence of tree-leaf temperatures. Nature 454:511–514.

Hennon PE, Beatty JS, Hildebrand D (2001) Hemlock dwarf mistletoe. Forest Insect and Disease Leaflet 135. USDA Forest Service, Forest Health Protection, Pacific Northwest Region, Portland, OR, USA.

Holmes RL (1983) Computer-assisted quality control in tree-ring dating and measurement. Tree Ring Bull 43:69–78.

Hubbard RM, Ryan MG, Stiller V, Sperry JS (2001) Stomatal conductance and photosynthesis vary linearly with plant hydraulic conductance in ponderosa pine. Plant Cell Environ 24:113–121.

Hull RJ, Leonard OA (1964) Physiological aspects of parasitism in mistletoes (*Arceuthobium* and *Phoradendron*). I. The carbohydrate nutrition of mistletoe. Plant Physiol 39:996–1007.

Kahmen A, Simonin K, Tu KP, Merchant A, Callister A, Siegwolf R, Dawson TE, Arndt SK (2008) Effects of environmental parameters, leaf physiological properties and leaf water relations on leaf water $\delta^{18}O$ enrichment in different Eucalyptus species. Plant Cell Environ 31:738–751.

Lambers H, Chapin FS III, Pons TL (2008) Plant physiological ecology. Springer, New York, USA.

Leavitt SW, Danzer SR (1993) Methods for batch processing small wood samples to holocellulose for stable-carbon isotope analysis. Anal Chem 65:87–89.

Leavitt SW, Long A (1982) Evidence for 13C/12C fractionation between tree leaves and wood. Nature 298:742–744.

Logan BA, Huhn ER, Tissue DT (2002) Photosynthetic characteristics of eastern dwarf mistletoe (*Arceuthobium pusillum* Peck) and its effects on the needles of host white spruce (*Picea glauca* [Moench] Voss). Plant Biol 4:740–745.

Logan BA, Reblin JS, Zonana DS et al. (2012) Impact of eastern dwarf mistletoe (*Arceuthobium pusillum*) on host white spruce (*Picea glauca*) development, growth and performance across multiple scales. Physiol Plant 147:502–513.

Marshall JD, Dawson TE, Ehleringer JR (1994*a*) Integrated nitrogen, carbon, and water relations of a xylem-tapping mistletoe following nitrogen fertilization of the host. Oecologia 100:430–438.

Marshall JD, Ehleringer JR, Schulze ED, Farquhar G (1994*b*) Carbon isotope composition, gas exchange and heterotrophy in Australian mistletoes. Funct Ecol 8:237–241.

Martin TA, Hinckley TM, Meinzer FC, Sprugel DG (1999) Boundary layer conductance, leaf temperature and transpiration of *Abies amabilis* branches. Tree Physiol 19:435–443.

McCarroll D, Loader NJ (2004) Stable isotopes in tree-rings. Quarternary Sci Rev 23:771–801.

McDowell NG, Bond BJ, Hill LT, Ryan MG, Whitehead D (2011) Relationships between tree height and carbon isotope discrimination. In: Meinzer FC, Lachenbruch B, Dawson TE (eds) Size- and age-related changes in tree structure and function. Springer, Dordrecht.

Meinzer FC, Woodruff DR, Shaw DC (2004) Integrated responses of hydraulic architecture, water and carbon relations of western hemlock to dwarf mistletoe infection. Plant Cell Environ 27:937–946.

Paw UKT, Gao W (1988) Applications of solutions to non-linear energy budget equations. Agric For Meteorol 43:121–145.

Reblin JS, Logan BA, Tissue DT (2006) Impact of eastern dwarf mistletoe (*Arceuthobium pusillum*) infection on the needles of red spruce (*Picea rubens*) and white spruce (*Picea glauca*): oxygen exchange, morphology and composition. Tree Physiol 26:1325–1332.

Roden JS, Ehleringer JR (2007) Summer precipitation influences the stable oxygen and carbon isotopic composition of tree-ring cellulose in *Pinus ponderosa*. Tree Physiol 27:491–501.

Roden JS, Farquhar GD (2012) A controlled test of the dual-isotope approach for the interpretation of stable carbon and oxygen isotope ratio variation in tree-rings. Tree Physiol 4:490–503.

Roden JS, Siegwolf R (2012) Is the dual-isotope conceptual model fully operational? Tree Physiol 32:1179–1182.

Roden JS, Lin G, Ehleringer JR (2000) A mechanistic model for interpretation of hydrogen and oxygen isotope ratios in tree-ring cellulose. Geochim Cosmochim Acta 64:21–35.

Sala A, Carey EV, Callaway RM (2001) Dwarf mistletoe affects whole-tree water relations of Douglas fir and western larch primarily through changes in leaf to sapwood ratios. Oecologia 126:42–52.

Sangüesa-Barreda G, Linares JC, Camarero JJ (2013) Drought and mistletoe reduce growth and water-use efficiency of Scots pine. For Ecol Manag 296:64–73.

Santiago LS, Goldstein G, Meinzer FC, Fisher JB, Machado K, Woodruff D, Jones T (2004) Leaf photosynthetic traits scale with hydraulic conductivity and wood density in Panamanian forest canopy trees. Oecologia 140:543–550.

Saurer M, Aellen K, Siegwolf R (1997) Correlating δ13C and δ18O in cellulose of trees. Plant Cell Environ 20:1543–1550.

Scheidegger Y, Saurer M, Bahn M, Siegwolf R (2000) Linking stable oxygen and carbon stable isotopes with stomatal conductance and photosynthetic capacity: a conceptual model. Oecologia 125:350–357.

Seibt U, Rajabi A, Griffiths H, Berry JA (2008) Carbon isotopes and water use efficiency: sense and sensitivity. Oecologia 155:441–454.

Sharkey TD, Bernacchi CJ, Farquhar GD, Singsaas EL (2007) Fitting photosynthetic carbon dioxide response curves for C3 leaves. Plant Cell Environ 30:1035–1040.

Shaw DC, Weiss SB (2000) Canopy light and the distribution of hemlock dwarf mistletoe aerial shoots in an old-growth Douglas-fir/western hemlock forest. Northwest Sci 74:306–315.

Shaw DC, Watson DM, Mathiasen RL (2004) Comparison of dwarf mistletoes (*Arceuthobium* spp., *Viscaceae*) in the western United States with mistletoes (*Amyema* spp., *Loranthaceae*) in Australia—ecological analogs and reciprocal models for ecosystem management. Aust J Bot 52:481–498.

Shaw DC, Chen J, Freeman EA, Braun DM (2005) Spatial and population characteristics of dwarf mistletoe infected trees in an old-growth Douglas-fir–western hemlock forest. Can J For Res 35:990–1001.

Shaw DC, Huso M, Bruner H (2008) Basal area growth impacts of dwarf mistletoe on western hemlock in an old-growth forest. Can J For Res 38:576–583.

Simard S, Morin H, Krause C, Buhay WM, Treydte K (2012) Tree-ring widths and isotopes of artificially defoliated balsam firs: a simulation of spruce budworm outbreaks in Eastern Canada. Environ Exp Bot 81:44–54.

Song X, Barbour MM, Farquhar GD, Vann DR, Helliker BR (2013) Transpiration rate relates to within- and across-species variations in effective pathlength in a leaf water model of oxygen isotope enrichment. Plant Cell Environ 36:1338–1351.

Stanton S (2007) Effects of dwarf mistletoe on climate response of mature ponderosa pine trees. Tree Ring Res 63:69–80.

Sternberg L (1989) Oxygen and hydrogen isotope measurements in plant cellulose analysis. In: Linskens HF, Jackson JF (eds) Modern methods of plant analysis, vol 10: plant fibers. Springer, Berlin, pp 89–99.

Terashima I, Hanba YT, Tazoe Y, Vyas P, Yano S (2006) Irradiance and phenotype: comparative eco-development of sun and shade leaves in relation to photosynthetic CO_2 diffusion. J Exp Bot 57:343–354.

Watson DM (2001) Mistletoe—a keystone resource in forests and woodlands worldwide. Annu Rev Ecol Evol Syst 32:219–249.

Way D (2011) Parasitic plants and forests: a climate change perspective. Tree Physiol 31:1–2.

Wilson CA, Calvin CL (1996) Anatomy of the dwarf mistletoe shoot system In: Hawksworth FG, Wiens D (eds) Dwarf mistletoes: biology, pathology, and systematics. USDA FS, Washington, DC, pp 95–111.

Woodruff DR, Meinzer FC, Lachenbruch B, Johnson DM (2009) Co-ordination of leaf structure and gas exchange along a height gradient in a tall conifer. Tree Physiol 29:261–272.

Yakir D, DeNiro MJ (1990) Oxygen and hydrogen isotope fractionation during cellulose metabolism in *Lemna gibba* L. Plant Physiol 93:325–332.

Zweifel R, Bangerter S, Rigling A, Sterck FJ (2012) Pine and mistletoes: how to live with a leak in the water flow and storage system? J Exp Bot 63:2565–2578.